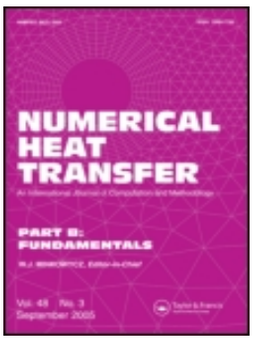

Numerical Heat Transfer, Part B: Fundamentals

ISSN: 1040-7790 (Print) 1521-0626 (Online) Journal homepage: http://www.tandfonline.com/loi/unhb20

The Atomistic Green's Function Method: An Efficient Simulation Approach for Nanoscale Phonon Transport

W. Zhang , T. S. Fisher & N. Mingo

To cite this article: W. Zhang , T. S. Fisher & N. Mingo (2007) The Atomistic Green's Function Method: An Efficient Simulation Approach for Nanoscale Phonon Transport, Numerical Heat Transfer, Part B: Fundamentals, 51:4, 333-349, DOI: 10.1080/10407790601144755

To link to this article: http://dx.doi.org/10.1080/10407790601144755

Numerical Heat Transfer, Part B, 51: 333–349, 2007

ISSN: 1040-7790 print/1521-0626 online
DOI: 10.1080/10407790601144755

Taylor & Francis
Taylor & Francis Group

THE ATOMISTIC GREEN'S FUNCTION METHOD: AN EFFICIENT SIMULATION APPROACH FOR NANOSCALE PHONON TRANSPORT

W. Zhang and T. S. Fisher
School of Mechancial Engineering and Birck Nanotechnology Center, Purdue University, West Lafayette, Indiana, USA

N. Mingo
NASA-Ames Center for Nanotechnology, 229-1, Moffett Field, California, USA

This article presents a general formulation of an atomistic Green's function (AGF) method. The atomistic Green's function approach combines atomic-scale fidelity with asymptotic treatment of large-scale (bulk) features, such that the method is particularly well suited to address an emerging class of multiscale transport problems. A detailed mathematical derivation of the phonon transmission function is provided in terms of Green's functions and, using the transmission function, the heat flux integral is written in Landauer form. Within this theoretical framework, the required inputs to calculate heat flux are equilibrium atomic locations and an appropriate interatomic potential. Relevant algorithmic and implementation details are discussed. Several examples including a homogeneous atomic chain and two heterogeneous atomic chains are included to illustrate the applications of this methodology.

INTRODUCTION

A growing interest exists in mesoscopic phonon transport, in which device dimensions becomes comparable to the typical wavelength of a phonon, and the wave nature of phonons becomes prominent. Meanwhile, the shrinking feature sizes of modern electronic and molecular devices are quickly approaching nanometer scales, and phonon transport is often restricted by the heterogeneous boundaries and interfaces embedded in devices. In this quasi-ballistic transport regime, the atomistic Green's function (AGF) method is efficient at handling interface and boundary scattering. In this article, we present a detailed mathematical derivation and a practical algorithm of the atomistic Green's function method, as well as examples of the numerical implementation of the method.

Quantized thermal transport has been investigated with a variety of methods of various degrees of complexity. Rego and Kirczenow [1] demonstrated theoretically that at low temperatures (<1 K) the thermal conductance of a one-dimensional quantum wire is quantized, and the fundamental quantum of thermal conductance is

Received 13 March 2006; accepted 3 November 2006.
Address correspondence to T. S. Fisher, School of Mechancial Engineering, Purdue University, 1205 West State Street, West Lafayette, IN 47907-2088, USA. E-mail: tsfisher@purdue.edu

NOMENCLATURE

A	matrix for convenience, defined in Eq. (15)
D	one-dimension phonon density of states, s/m
E	energy associated with degrees of freedom, J
g	uncoupled green's function matrix, defined in Eqs. (9) and (10)
G	green's function matrix, defined in Eq. (11)
h	Planck constant ($=6.63\times10^{-34}$ m^2 kg/s)
$\hbar$	reduced Planck constant ($=h/2\pi$)
H	harmonic matrix, defined in Eq. (1)
i	unitary imaginary number
I	identity matrix
J	energy flux, W
k_B	Boltzmann constant ($=1.38\times10^{-23}$ m^2 kg/s^2 K)
L	bond length, m
M	atomic mass, kg
n	matrix dimension
N	phonon occupation number
S	source matrix, defined in Eq. (12)
t	time, s
T	temperature, K
u	vibrational degree of freedom on displacement, m
ũ	column vector consisting of vibrational degrees of freedom
U	interatomic potential, J
Γ	matrix for convenience, denned in Eq. (16)
δ	a small number corresponding to phonon energy dissipation in contacts
ϵ	a quantity defined as ω^2
σ	thermal conductance, W/K
Σ	self-energy matrix, defined in Eq. (11)
τ	matrix representing interactions among different atom groups
ϕ	complex wave function
Φ	column vector representing vibrational degrees of freedom in either contact
χ	column vector representing the change to the original vector Φ^R after contacts and the device are connected
ψ	column vector representing vibrational degrees of freedom in the connected device
ω	angular frequency, rad/s

Subscripts and Superscripts

c	contact region
cd	connection between contact region and device region
d	device region including LD, RD, and D
D	device region not directly bonding with either contact
l	local density of states
LC	left contact region
LCB	left contact bulk region
LD	left Device region
m	degree of freedom running index
p	matrix row index, or the index of a degree of freedom
q	matrix column index, or the index of a degree of freedom
R	disconnected state
RC	right contact region
RCB	right Contact bulk region
RD	right device region
s	submatrix
*	complex conjugate of a matrix
†	conjugate transpose of a matrix

$\pi^2k_B^2T/3h$, regardless of material properties. Similar work on an atomic chain using a Keldysh formalism was presented by Ozpineci and Ciraci [2]. Hyldgaard [3] applied the lattice dynamics method, developed earlier by Pettersson and Mahan [4] and by Stoner and Maris [5], to a one-dimensional lattice model with single-barrier and double-barrier structural configurations. Hyldgaard's investigation shows the effect of phonon Fabry-Perot resonances on thermal conductance.

At low temperatures, the phonon distribution is shifted to the long-wavelength portion of the spectrum; therefore acoustic theory suffices to study transport phenomena. The transmission coefficient for vibrational waves traveling across an abrupt junction between two thin elastic plates can be calculated by the thin-plate elasticity theory described by Cross and Lifshitz [6]. Surface roughness effects

phonon scattering on thermal conductance have been calculated with a full elasticity theory [7–9] in an attempt to explain why the ratio of thermal conductance to temperature decreases at extremely low temperatures [10]. A scattering-matrix method with a continuum elastic wave model was developed by Li et al. [11] to evaluate the thermal conductance of a dielectric quantum wire. This method was later extended to investigate the effects of discontinuities [12] and defects [13] in crystal lattices. The limitations of the acoustic type of approach are its inability to handle exact atomic structures and its neglect of other phonon branches.

Many other theoretical and numerical tools have been developed to simulate micro/nanoscale phonon transport and include molecular dynamics (MD) [14, 15] and the phonon Boltzmann transport equation (BTE) [16, 17]. Compared to these methods, the atomistic Green's function method is strictly valid at low temperatures. It accounts for boundary and interface scattering efficiently and offers great flexibility in handling complicated geometries.

In a typical device-contact setup, contacts (or thermal reservoirs) play significant roles. Phonon distributions in contacts can significantly change the phonon transport characteristics of the device [18]. A well-designed device-contact geometric connection for ideal coupling was used in pioneering low-temperature thermal conductance measurements by Schwab et al. [10] in which the thermal quantum conductance was experimentally verified. The AGF method uses self-energy matrices to represent the effect of bulk contacts on the device, thus simplifying the complexities of multiscale transport.

Interface and boundary scattering processes are becoming increasingly important in practical devices. Two primary theories have been employed to explain the mechanism of the thermal boundary resistance. One is the acoustic mismatch model (AMM) by Little [19], and the other is the diffuse mismatch model (DMM) by Swartz and Pohl [20]. Both models neglect atomic details of actual interfaces, and thus offer limited accuracy in nanoscale interface resistance predictions [21]. The AGF method can predict thermal boundary resistance between heterogeneous materials with full consideration of the interfacial atomic structures.

Inspired by the success of the Green's function method in nanoscale electron transport simulations [22–24], we have investigated ballistic phonon transport in several practical configurations using the atomistic Green's function method [25–27]. In spite of a few previous publications, we believe that an article dedicated to AGF theory and algorithm details will facilitate the adoption of this method by a broader community.

In the first part of this article, a mathematical derivation starting from the lattice dynamic equation is described, and the phonon transmission function is expressed in terms of Green's functions. Relevant details of numerical implementation are discussed in the subsequent section. Several demonstrative atomic chain examples are presented to show the applicability of the method.

MATHEMATICAL FORMULATION

General Problem Description

The common atomic structure of interest can be generalized as a device between two contacts, as shown in Figure 1. "Contact1" (including atom groups

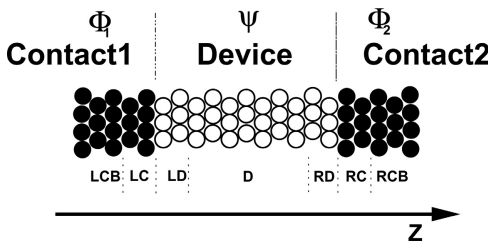

Figure 1. Schematic diagram for a general contact-device-contact setup.

LCB and LC) and "Contact2" (including atom groups RCB and RC) are two semi-infinite thermal reservoirs at constant temperatures T_1 and T_2, respectively. The "Device" includes atom groups LD, D, and RD, and its geometry is arbitrary (e.g., an atomic chain, a nanowire, or a thin film). The types of connections between the device and contacts are arbitrary also (e.g., point contact, limited contact, or planar contact). Atom group LC includes atoms in "Contact1" that bond with "Device" atoms. Atoms in group LCB do not have any bonds with "Device" atoms. Therefore, the dynamical properties of these two groups (LCB and LC) will be different in a general heterogeneous system. Similar definitions are extended to atom groups RC and RCB. Atom groups LD and RD include "Device" atoms that bond with "Contact1" and "Contact2" atoms, respectively. Atoms in group D have no bonds with either contact.

Harmonic Matrix

The AGF method is founded on a harmonic matrix for the system of interest. Prior work [26] has shown that anharmonic scattering can generally be neglected at room temperature if the characteristic length of the device is less than 20 nm. Therefore, a harmonic matrix can be used to represent interactions among different degrees of freedom. The mathematical definition of the harmonic matrix is[1]

$$\mathbf{H} = \{H_{pq}\} = \frac{1}{\sqrt{M_p M_q}} \begin{cases} -\frac{\partial^2 U}{\partial u_p \partial u_q} & \text{if } p \neq q \\ -\sum\limits_{\mathrm{m} \neq \mathrm{q}} \frac{\partial^2 U}{\partial u_q \partial u_m} & \text{if } p = q \end{cases} \tag{1}$$

where u_p and u_q refer to any two atomic vibrational degrees of freedom (i.e., displacements), respectively. U represents the total interatomic potential. M_p and M_q are atomic masses associated with degrees of freedom u_P and u_q, respectively. The dynamical equation for the system of interest can be written as [28]

$$(\omega^2 \mathbf{I} - \mathbf{H})\tilde{\boldsymbol{u}} = 0 \tag{2}$$

[1]In this article, all summations are explicit, i.e., no Einstein summation rule is used.

where $\tilde{u}$ is a column vector consisting of vibrational degrees of freedom. We note that in some complicated situations, the assembled harmonic matrix $\mathbf{H}$ can contain complex entries, but it is always a Hermitian matrix and thus has only real eigenvalues.

Green's Function Matrices

In this article, we use matrices τ_1 and τ_2 to represent interactions between two different atom groups. A column vector ψ represents vibrational degrees of freedom in the device, and Φ, another column vector, represents vibrational degrees of freedom in either contact. The number of degrees of freedom in the contact approaches infinity, and we therefore use a sufficiently large number n_c to approximate the number of degrees of freedom in the contact. The number of degrees of freedom in the device is finite and termed as n_d. The number of degrees of freedom in interface regions (LC, LD, RC, and RD) is n_{cd}. Based on Eq. (2), the dynamical equations of the disconnected contacts are

$$[\omega^2\mathbf{I} - \mathbf{H_1}]\Phi_1^R = 0 \tag{3}$$

$$[\omega^2\mathbf{I} - \mathbf{H_2}]\Phi_2^R = 0 \tag{4}$$

where $\mathbf{H}_1$ and $\mathbf{H}_2$ are harmonic matrices of the two contacts. The superscript R refers to the disconnected state. Using χ as the change to the original contact vector (Φ^R) after the contact and device are connected, the actual contact vector is $\Phi = \Phi^R + \chi$. The dynamical equation of the connected contacts and device is then

$$\begin{bmatrix} \omega^2\mathbf{I} - \mathbf{H}_1 & -\tau_1^\dagger & 0 \\ -\tau_1 & \omega^2\mathbf{I} - \mathbf{H}_d & -\tau_2 \\ 0 & -\tau_2^\dagger & \omega^2\mathbf{I} - \mathbf{H}_2 \end{bmatrix} \begin{Bmatrix} \Phi_1^R + \chi_1 \\ \psi \\ \Phi_2^R + \chi_2 \end{Bmatrix} = 0 \tag{5}$$

where τ_1 (or τ_2) is the connection matrix between the left (or right) contact and the device. The solutions to Eq. (5) can be written as [24]

$$\chi_1 = \mathbf{g}_1\tau_1^\dagger\psi \tag{6}$$

$$\chi_2 = \mathbf{g}_2\tau_2^\dagger\psi \tag{7}$$

$$\psi = \mathrm{GS} \tag{8}$$

The matrices used in Eqs. (6), (7), and (8) are defined as

$$\mathbf{g}_1 = \lim_{\delta\to 0}[(\omega^2 + \delta i)\mathbf{I} - \mathbf{H}_1]^{-1} \qquad \text{(uncoupled Green's function)} \tag{9}$$

$$\mathbf{g}_2 = \lim_{\delta\to 0}[(\omega^2 + \delta i)\mathbf{I} - \mathbf{H}_2]^{-1} \qquad \text{(uncoupled Green's function)} \tag{10}$$

$$\mathbf{G} = \left[\omega^2\mathbf{I} - \mathbf{H}_d - \underbrace{\tau_1\mathbf{g}_1\tau_1^\dagger}_{\Sigma_1} - \underbrace{\tau_2\mathbf{g}_2\tau_2^\dagger}_{\Sigma_2}\right]^{-1} \qquad \text{(Green's function)} \tag{11}$$

$$\mathbf{S} = \underbrace{\tau_1\Phi_1^R}_{\mathbf{S}_1} + \underbrace{\tau_2\Phi_2^R}_{\mathbf{S}_2} \tag{12}$$

where i is the unitary imaginary number. The importance of the perturbation δ is addressed in the following section. These solutions can be easily verified by back-substituting them into Eq. (5).

$$\mathbf{S}_1\mathbf{S}_2^\dagger = \tau_1\Phi_1^R\Phi_2^{R\dagger}\tau_2^\dagger = 0 \tag{13}$$

$$\mathbf{S}_2\mathbf{S}_1^\dagger = \tau_2\Phi_2^R\Phi_1^{R\dagger}\tau_1^\dagger = 0 \tag{14}$$

because Φ_1^R and Φ_2^R are degree of freedom vectors of the two disconnected contacts with null inner products. Several matrices used later for convenience are also defined as

$$\mathbf{A} = i[\mathbf{G} - \mathbf{G}^\dagger] = \underbrace{i[\mathbf{g}_1 - \mathbf{g}_1^\dagger]}_{\mathbf{A}_1} + \underbrace{i[\mathbf{g}_2 - \mathbf{g}_2^\dagger]}_{\mathbf{A}_2} = \underbrace{\mathbf{G}\Gamma_1\mathbf{G}^\dagger}_{\mathbf{A}_1} + \underbrace{\mathbf{G}\Gamma_2\mathbf{G}^\dagger}_{\mathbf{A}_2} \tag{15}$$

$$\Gamma = \underbrace{\tau_1\mathbf{A}_1\tau_1^\dagger}_{\Gamma_1} + \underbrace{\tau_2\mathbf{A}_2\tau_2^\dagger}_{\Gamma_2} \tag{16}$$

and the proof of Eqs. (15) and (16) can be found in [24].

Energy Flux Between any Two Degrees of Freedom

The energy associated with any degree of freedom consists of kinetic and potential energies,

$$E_p = \frac{1}{4}\sum_q (u_p^* k_{pq} u_q + u_q^* k_{qp} u_p) + \frac{M_p}{2}\dot{u}_p^* \cdot \dot{u}_p \tag{17}$$

where

$$k_{pq} = H_{pq}\sqrt{M_p M_q} \tag{18}$$

The time derivative of this energy (E_p) is

$$\frac{dE_p}{dt} = \frac{1}{4}\sum_q (\dot{u}_p^* k_{pq} u_q + u_p^* k_{pq}\dot{u}_q + \dot{u}_q^* k_{qp} u_p + u_q^* k_{qp}\dot{u}_p) + \frac{M_p}{2}(\ddot{u}_p^*\dot{u}_p + \dot{u}_p^*\ddot{u}_p) \tag{19}$$

Using Newton's second law ($M_p\ddot{u}_p = -\Sigma_q k_{pq}u_q$ and $M_p\ddot{u}_p^* = -\Sigma_q k_{qp}u_q^*$), Eq. (19) can be expressed as

$$\frac{dE_p}{dt} = \frac{1}{4}\sum_q (u_p^* k_{pq}\dot{u}_q + \dot{u}_q^* k_{qp}u_p - u_q^* k_{qp}\dot{u}_p - \dot{u}_p^* k_{pq}u_q) \tag{20}$$

The expressions $u_p = \phi_p e^{-iwt}/\sqrt{M_p}$ and $u_q = \phi_q e^{-iwt}/\sqrt{M_q}$ (ϕ_p and ϕ_q with no time dependence) simflify Eq. (20) to

$$\frac{dE_p}{dt} = \frac{\omega}{2i}\sum_q \left[\phi_p^* H_{pq}\phi_q - \phi_q^* H_{qp}\phi_p\right] \equiv \sum_q J_{pq} \tag{21}$$

Equation (21) takes a typical form of an energy conservation equation, and accordingly, it is natural to define the energy flux between any two degrees of freedom (u_p and u_q) as

$$J_{pq} = \frac{\omega}{2i}\left[\phi_p^* H_{pq}\phi_q - \phi_q^* H_{qp}^*\phi_p\right] \tag{22}$$

Normalization

Using Eq. (17) and $u_p = \phi_p e^{-iwt}/\sqrt{M_p}$, the normalization condition for phonons can be expressed as

$$\begin{aligned}\hbar\omega &= \sum_p E_p \\ &= \sum_p \left[\frac{1}{4}\sum_q (u_p^* k_{pq}u_q + u_q^* k_{qp}u_p) + \frac{M_p}{2}\dot{u}_p^* \cdot \dot{u}_p\right] \\ &= \sum_p \omega^2 |\phi_p|^2\end{aligned} \tag{23}$$

Therefore

$$\sum_p |\phi_p|^2 = \frac{\hbar}{\omega}, \text{or} \sum_p \left|\frac{\phi_p}{\sqrt{\hbar/\omega}}\right|^2 = 1 \tag{24}$$

The Expression for Total Energy Flux

Total energy flux is the summation of fluxes between individual degrees of freedom following Eq. (22). J_1, the heat flux between "Contactl" and "Device," is expressed as

$$\begin{aligned}J_1 &= \frac{\omega\,\text{Trace}\left[\psi^\dagger\tau_1\Phi_1 - \Phi_1^\dagger\tau_1^\dagger\psi\right]}{2i} \\ &= \underbrace{\frac{\omega\,\text{Trace}\left[\psi^\dagger\tau_1\Phi_1^R - \Phi_1^{R\dagger}\tau_1^\dagger\psi\right]}{2i}}_{\text{Inflow}} - \underbrace{\frac{\omega\,\text{Trace}\left[\chi_1^\dagger\tau_1^\dagger\psi - \psi^\dagger\tau_1\chi_1\right]}{2i}}_{\text{out flow}}\end{aligned} \tag{25}$$

where we have used the fact that the trace of any matrix product is independent of the order of multiplication. Using Eqs. (6), (7), (8), (12), (13), and (14), the inflow term can be written as

$$\begin{aligned}\text{Inflow} &= \frac{\omega\,\text{Trace}\left[\mathbf{S}^{\dagger}\mathbf{G}^{\dagger}\mathbf{S}_{\mathbf{1}} - \mathbf{S}_{\mathbf{1}}^{\dagger}\mathbf{G}\mathbf{S}\right]}{2i} \\ &= \frac{\omega\,\text{Trace}\left[\mathbf{S}_{\mathbf{1}}\mathbf{S}_{\mathbf{1}}^{\dagger}\mathbf{G}^{\dagger} - \mathbf{S}_{\mathbf{1}}\mathbf{S}_{\mathbf{1}}^{\dagger}\mathbf{G}\right]}{2i} \\ &= \frac{\omega\,\text{Trace}\left[\mathbf{S}_{\mathbf{1}}\mathbf{S}_{\mathbf{1}}^{\dagger}\mathbf{A}\right]}{2}\end{aligned} \tag{26}$$

With the normalization condition in Eq. (24), we can express the number of phonons in terms of matrix A_1, which relates to the Green's function matrix [see Eq. (15)]

$$\omega\Phi_1^{R\dagger}\Phi_1^R \Rightarrow \int \frac{\hbar}{2\pi} N_1(\varepsilon)\mathbf{A}_1\, d\varepsilon \tag{27}$$

where $\varepsilon = \omega^2$. Therefore

$$\omega\mathbf{S}_1\mathbf{S}_1^{\dagger} = \omega\tau_1\Phi_1^R\Phi_1^{R\dagger}\tau_1^{\dagger} \Rightarrow \int \frac{\hbar}{2\pi} N_1(\varepsilon)\tau_1\mathbf{A}_1\tau_1^{\dagger}\, d\varepsilon = \int \frac{\hbar}{2\pi} N_1(\varepsilon)\Gamma_1\, d\varepsilon \tag{28}$$

where $N_1(\varepsilon)$ is the number of phonons in "Contact 1" at the eigenstate $\varepsilon = \omega^2$. Combining Eqs. (26) and (28), we have

$$\text{Inflow} = \int \frac{\hbar\omega}{2\pi} N_1(\omega)\text{Trace}(\Gamma_1\mathbf{A})\, d\omega \tag{29}$$

The outflow term in Eq. (25) can be evaluated using Eq. (8):

$$\begin{aligned}\text{Outflow} &= \frac{\omega\,\text{Trace}[\psi^{\dagger}\tau_1\mathbf{g}_1^{\dagger}\tau_1^{\dagger}\psi - \psi^{\dagger}\tau_1\mathbf{g}_1\tau_1^{\dagger}\psi]}{2i} \\ &= \frac{\omega\,\text{Trace}[\mathbf{S}^{\dagger}\mathbf{G}^{\dagger}\mathbf{G}\mathbf{S}(\tau_1\mathbf{g}_1^{\dagger}\tau_1^{\dagger} - \tau_1\mathbf{g}_1\tau_1^{\dagger})]}{2i} \\ &= \frac{\omega\,\text{Trace}[\mathbf{G}\mathbf{S}\mathbf{S}^{\dagger}\mathbf{G}^{\dagger}\Gamma_1]}{2i}\end{aligned} \tag{30}$$

Combining Eqs. (12), (13), and (14), we find

$$\begin{aligned}\omega\mathbf{S}\mathbf{S}^{\dagger} &= \omega\mathbf{S}_1\mathbf{S}_1 + \omega\mathbf{S}_2\mathbf{S}_2 \\ &\Rightarrow \int \frac{\hbar}{2\pi} N_1(\varepsilon)\tau_1\mathbf{A}_1\tau_1^{\dagger}\, d\varepsilon + \int \frac{\hbar}{2\pi} N_2(\varepsilon)\tau_2\mathbf{A}_2\tau_2^{\dagger}\, d\varepsilon \\ &= \int \frac{\hbar}{2\pi} N_1(\varepsilon)\Gamma_1\, d\varepsilon + \int \frac{\hbar}{2\pi} N_2(\varepsilon)\Gamma_2\, d\varepsilon\end{aligned} \tag{31}$$

Therefore, the outflow term, becomes

$$\begin{aligned}\text{Outflow} &= \int \frac{\hbar\omega}{2\pi}\,\text{Trace}[\mathbf{G}(N_1(\omega)\Gamma_1 + N_2(\omega)\Gamma_2)\mathbf{G}^\dagger\Gamma_1]\,d\omega \\ &= \int \frac{\hbar\omega}{2\pi}\,\text{Trace}[N_1(\omega)\mathbf{A}_1\Gamma_1 + N_2(\omega)\mathbf{A}_2\Gamma_1]\,d\omega \end{aligned} \tag{32}$$

The total energy flux between "Contact 1" and "Device" is then

$$\begin{aligned} J_1 &= \int \frac{\hbar\omega}{2\pi}\{\text{Trace}[\Gamma_1\mathbf{A}]N_1(\omega) - \text{Trace}[N_1(\omega)\mathbf{A}_1\Gamma_1 + N_2(\omega)\mathbf{A}_2\Gamma_1]\}\,d\omega \\ &= \int \frac{\hbar\omega}{2\pi}\text{Trace}[\Gamma_1\mathbf{A}_2][N_1(\omega) - N_2(\omega)]\,d\omega \\ &= \int \frac{\hbar\omega}{2\pi}\text{Trace}[\Gamma_1\mathbf{G}\Gamma_2\mathbf{G}^\dagger][N_1(\omega) - N_2(\omega)]\,d\omega \end{aligned} \tag{33}$$

In the same manner, the total energy flux between "Contact 2" and "Device" is expressed as

$$\begin{aligned} J_2 &= \int \frac{\hbar\omega}{2\pi}\text{Trace}[\Gamma_2\mathbf{A}_1][N_2(\omega) - N_1(\omega)]\,d\omega \\ &= \int \frac{\hbar\omega}{2\pi}\text{Trace}[\Gamma_2\mathbf{G}\Gamma_1\mathbf{G}^\dagger][N_2(\omega) - N_1(\omega)]\,d\omega \end{aligned} \tag{34}$$

At steady state, J_1 equals $-J_2$ because

$$\begin{gathered} \text{Trace}[\Gamma_1\mathbf{A}] = \text{Trace}[\Gamma_1\mathbf{G}^\dagger\Gamma\mathbf{G}] = \text{Trace}[\Gamma\mathbf{G}^\dagger\Gamma_1\mathbf{G}] = \text{Trace}[\Gamma\mathbf{A}_1] \\ \text{Trace}[\Gamma_1\mathbf{A} - \Gamma_1\mathbf{A}_1] = \text{Trace}[\Gamma\mathbf{A}_1 - \Gamma_1\mathbf{A}_1] \\ \text{Trace}[\Gamma_1\mathbf{A}_2] = \text{Trace}[\Gamma_2\mathbf{A}_1] \end{gathered} \tag{35}$$

Finally, the heat flux can be written in Landauer form [29] as

$$J = \int \frac{\hbar\omega}{2\pi}\Xi(\omega)[N_1(\omega) - N_2(\omega)]\,d\omega \tag{36}$$

where the transmission function is

$$\Xi(\omega) = \text{Trace}[\Gamma_1\mathbf{G}\Gamma_2\mathbf{G}^\dagger] = \text{Trace}[\Gamma_2\mathbf{G}\Gamma_1\mathbf{G}^\dagger] \tag{37}$$

and thermal conductance (σ) is the ratio of heat flux J to the temperature difference,

$$\sigma = \frac{J}{\Delta T} \tag{38}$$

NUMERICAL IMPLEMENTATION

An algorithmic flow chart for the atomistic Green's function method is shown in Figure 2. The first step involves constructing the harmonic matrix

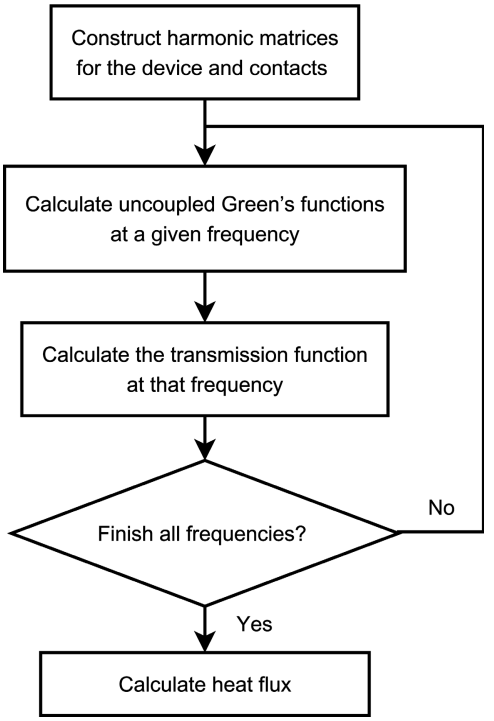

Figure 2. Algorithmic flow chart for the atomistic Green's function method.

based on Eq. (1). The evaluation process can be either numerical (for a complicated potential) or analytical (for a simple potential), provided that atomic locations and interatomic potential parameters are known. The second step involves calculating the uncoupled Green's functions $\mathbf{g}_1$ and $\mathbf{g}_2$. The size of $\mathbf{g}_1$ or $\mathbf{g}_2$ $(n_c \times n_c)$ is typically substantial because of their physical sizes. However, in the transmission calculation, $\mathbf{g}_1$ always appears in the form $\tau_1 \mathbf{g}_1 \tau_1^{\dagger}$, and τ_1 has only a finite number of nonzero elements. These nonzero elements comprise a submatrix τ_1^s that physically represents interactions between LC and LD. Therefore τ_1^s has a finite size of $n_{cd} \times n_{cd}$, as does τ_2^s. Consequently, the significant part of $\mathbf{g}_1$ is its submatrix $\mathbf{g}_1^s$ $(n_{cd} \times n_{cd})$ that corresponds to atoms in LC. The significant part of $\mathbf{g}_2$ is also its submatrix $\mathbf{g}_2^s$ $(n_{cd} \times n_{cd})$ that corresponds to atoms in RC.

Therefore, computational savings can be achieved by considering only these parts of $\mathbf{g}_1$ and $\mathbf{g}_2$. The decimation technique [30] is typically employed to calculate $\mathbf{g}_1^s$ and $\mathbf{g}_2^s$ because of its computational efficiency and low memory requirements. If the contact is homogeneous, i.e., if LCB and LC have identical dynamical properties, the decimation technique can be used directly. Otherwise, an additional calculation is needed as discussed later.

Another issue that deserves discussion is the selection of δ, which is a small number corresponding to phonon energy dissipation in contacts, whose role is

elaborated in [24]. We recommend that δ take the following general form:

$$\delta = f(\omega)\omega^2 \tag{39}$$

where $f(\omega)$ is a monotonically decreasing function. We select $f(\omega) = 0.001(1 - \omega/\omega_{\max})$, where $\omega_{\max}$ is the maximum phonon vibrational frequency. The choice of δ affects the energy resolution in the uncoupled Green's function and subsequent calculations. A smaller δ value gives better energy resolution but requires longer computational times.

The last numerical concern involves the significantly large number of matrix inversions in the calculation of Green's functions. A fast algorithm can be applied because all harmonic matrices have banded structures, and banded-matrix inversion is not as expensive numerically as direct inversion [31]. We also note that only a subset of entries in the Green's function **G** requires evaluation because only nonzero elements in Γ_1 and Γ_2 are significant in the final transmission formula [see Eq. (37)]. Additional computational saving can be achieved by evaluating only the significant part of **G**. However, we have observed that in some rare cases, the matrix condition number of $[\omega^2\mathbf{I} - \mathbf{H}_d - \Sigma_1 - \Sigma_2]$ is sufficiently large, in which case special care needs to be exerted to obtain the significant part of **G**.

RESULTS AND DISCUSSION

Homogeneous Atomic Chain

A homogeneous atomic chain is employed to demonstrate the AGF method and is shown in Figure 3*a* with one degree of freedom per atom. We have selected three atoms to constitute the "Device" region, and only nearest-neighbor atomic interactions are considered. The chosen bond strength (i.e., the spring constant) is 32 N/m, approximately equal to the bond strength in silicon. The atomic mass and spacing are 4.6×10^{-26} kg and 5.5 Å, respectively. In this case, the dynamical properties of LCB and LC are the same, so the decimation technique can be used

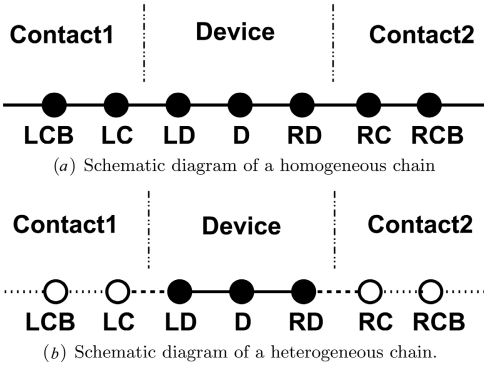

(*a*) Schematic diagram of a homogeneous chain

(*b*) Schematic diagram of a heterogeneous chain.

Figure 3. Homogeneous and heterogeneous atomic chain examples. Filled and open circles represent different types of atoms. The dotted, dashed, and solid lines between atoms represent different bonds.

directly to obtain uncoupled Green's functions. Analytical solutions for the uncoupled Green's functions $\mathbf{g}_1^s$ and $\mathbf{g}_2^s$ in this simple case can be found in the [32].

The atomistic Green's function method does not require *a priori* knowledge of phonon dispersion curves or density of states. Instead, it can be used to calculate the local density of states on each atom in the system. In the case of a one-dimensional atomic chain, the local density of states matrix (LDOS: D_l) is associated directly with the local Green's function ($\mathbf{G}$):

$$\mathbf{D}_l = \frac{i(\mathbf{G} - \mathbf{G}^\dagger)\omega}{\pi L} \tag{40}$$

where L is the bond length. The exact local density of states on the ith degree of freedom will correspond to the ith diagonal element of $\mathbf{D}_l$. The global density of states function is the same as the local density of states in homogeneous materials, and it is shown in Figure 4 together with the theoretical phonon density of states in a homogeneous atomic chain [33]. A cutoff frequency exists and sets an upper frequency.

The full-spectrum transmission function of the homogeneous chain is calculated using the atomistic Green's function method, and the result is shown in Figure 5. The transmission is unity at all frequencies below the cutoff frequency (a consequence of the harmonic assumption), and the transmission becomes zero at frequencies above the cutoff frequency because the phonon density of states is zero at these frequencies.

Heterogeneous Atomic Chain

Simulation of a heterogeneous atomic chain provides more physical insights as compared to a homogeneous atomic chain. A heterogeneous atomic chain configuration

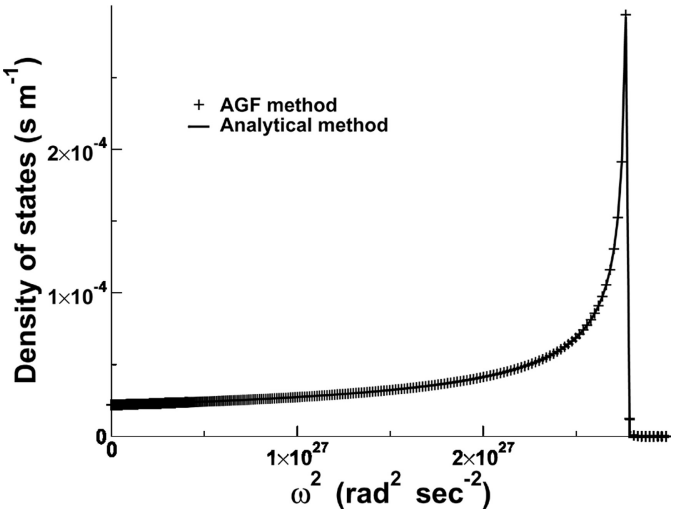

Figure 4. Comparison of density of states functions in a homogeneous atomic chain calculated by the AGF method and an analytical method [33].

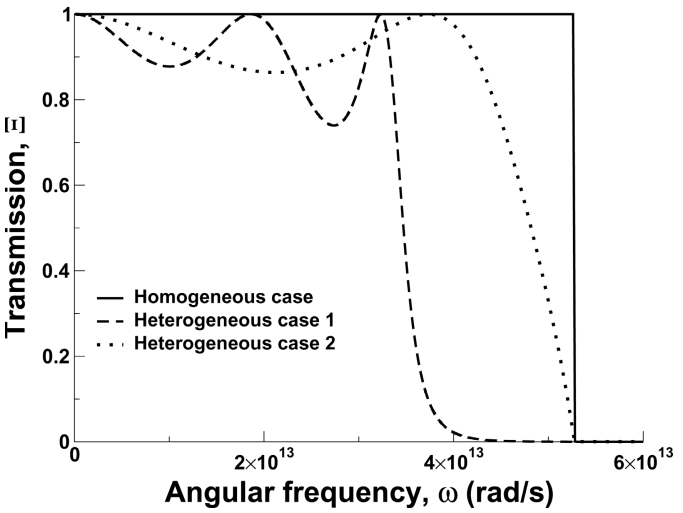

Figure 5. Comparison of transmission functions for homogeneous and heterogeneous atomic chains. The mass of a "Device" atom in the homogeneous case is 4.6×10^{-26} kg. The masses of "Device" atoms in the two heterogeneous cases are 9.2 and 2.3×10^{-26} kg, respectively.

is shown in Figure 3*b*, with one degree of freedom per atom. One additional step is needed to calculate $\mathbf{g}_1^s$ and $\mathbf{g}_2^s$:

$$\mathbf{g}_1^s = [(\omega^2 + \delta_i)\mathbf{I} - \mathbf{H}_{LC} - \tau_{LC,LCB}\mathbf{g}_{LCB}\tau_{LCB,LC}]^{-1} \tag{41}$$

$$\mathbf{g}_2^s = [(\omega^2 + \delta_i)\mathbf{I} - \mathbf{H}_{RC} - \tau_{RC,RCB}\mathbf{g}_{RCB}\tau_{RCB,RC}]^{-1} \tag{42}$$

where $\mathbf{g}_{LCB}$ and $\mathbf{g}_{RCB}$ are uncoupled Green's functions for LCB and RCB, respectively, and they are obtained from the decimation technique. $\mathbf{H}_{LC}$ and $\mathbf{H}_{RC}$ are harmonic matrices for LC and RC, respectively. $\tau_{LC,LCB}$ and $\tau_{LCB,LC}$ are matrices that connect LC and LCB ($\tau_{LC,LCB} = \tau_{LCB,LC}^{\dagger}$), and $\tau_{RC,RCB}$ and $\tau_{RCB,RC}$ are matrices that connect RC and RCB ($\tau_{RC,RCB} = \tau_{RCB,RC}^{\dagger}$).

The ratios between spring constants and atomic masses dictates the harmonic matrix and thus the thermal conductance. Therefore, the effect of doubling the spring contact is equal to the effect of reducing the the atomic mass by half, except for the interfacial atoms. To simplify the discussion, only the atomic masses of "Device" atoms are changed in the two heterogeneous cases, which conceptually can be thought of as isotopes. The properties of "Contact" atoms remain the same as those in the homogeneous chain case. The atomic masses are 9.2×10^{-26} kg and 2.3×10^{-26} kg in the first and second heterogeneous cases, respectively. The bond strength between a "Device" atom and a "Contact" atom, though unchanged in these two specific cases, takes the mean value of "Device" atoms and "Contact" atoms if necessary.

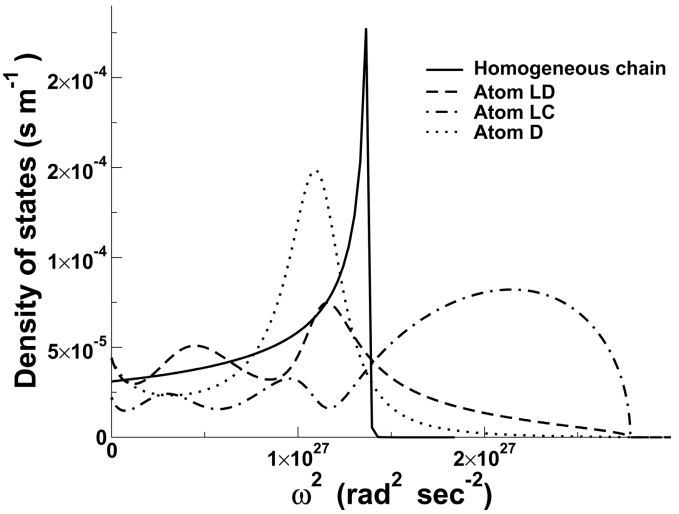

Figure 6. The local density of states functions at various locations, compared to the density of states function of the homogeneous chain made of "Device" atoms. The mass of "Device" atoms in the homogeneous case is 4.6×10^{-26} kg. The masses of "Device" atoms in the two heterogeneous cases are 9.2 and 2.3×10^{-26} kg, respectively.

The local phonon density of states in any heterogeneous chain differs from the global density of states in a bulk solid. For the first heterogeneous case (device atomic mass $= 9.2 \times 10^{-26}$ kg), the LDOS functions of atoms LC, LD, and D are shown in Figure 6 along with the bulk density of states of "Device" atoms. The LDOS functions of atoms RC and RD are the same as those of LC and LD, because of the symmetric configuration, and thus they are not shown. The LDOS functions exhibit pronounced differences with the bulk density of states resulted from the coupling between the device and the contacts.

The transmission functions in the two heterogeneous cases are compared to that of the homogeneous atomic chain in Figure 5. At extremely low frequencies, the heterogeneous chain exhibits the same transmission as the homogeneous chain because the long wavelengths of low-frequency phonons limit the influence of the boundary scattering. However, at higher frequencies, phonons are scattered by heterogeneous interfaces, causing decreased transmission. Several Fabry-Perot peaks, where the transmission function reaches unity, are observed due to the resonant scattering of phonons.

The thermal conductances of the homogeneous and heterogeneous cases are compared in Figure 7. Due to interface scattering, the heterogeneous atomic chain exhibits a smaller conductance than the homogeneous atomic chain over all temperature ranges. However, at low temperatures, minimal differences exist among conductances of homogeneous and heterogeneous cases because of the convergence of transmission functions at low frequencies. The conductances of both homogeneous and heterogeneous systems exhibit a linear temperature dependence at low temperatures.

Lastly, we nondimensionalize thermal conductance as the ratio of the thermal conductance (σ) to the quantum conductance ($\pi^2 k_B^2 T/3h$). The quantum conductance is the conductance on a homogeneous atomic chain with infinitely large bond

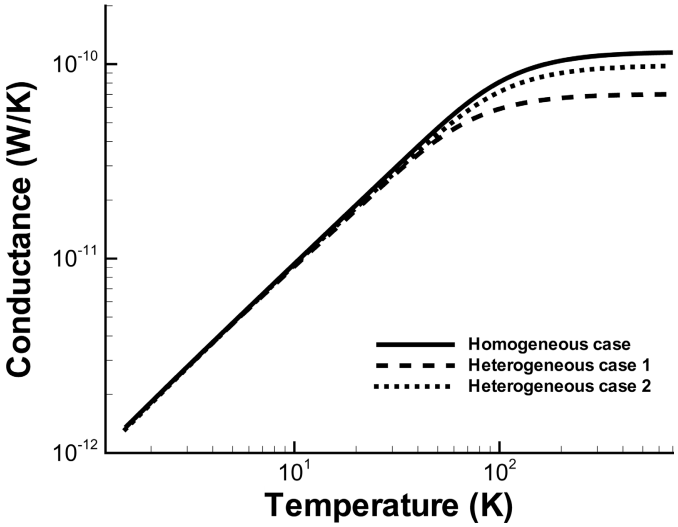

Figure 7. Comparison of thermal conductances for homogeneous and heterogeneous atomic chains. The mass of a "Device" atom in the homogeneous case is 4.6×10^{-26} kg. The masses of "Device" atoms in the two heterogeneous cases are 9.2 and 2.3×10^{-26} kg, respectively.

strength or infinitesimal atomic masses. Thus, the nondimensional conductance indicates how well each test case represents an ideal phonon conductor. The length dependencies of the nondimensional thermal conductances at different temperatures

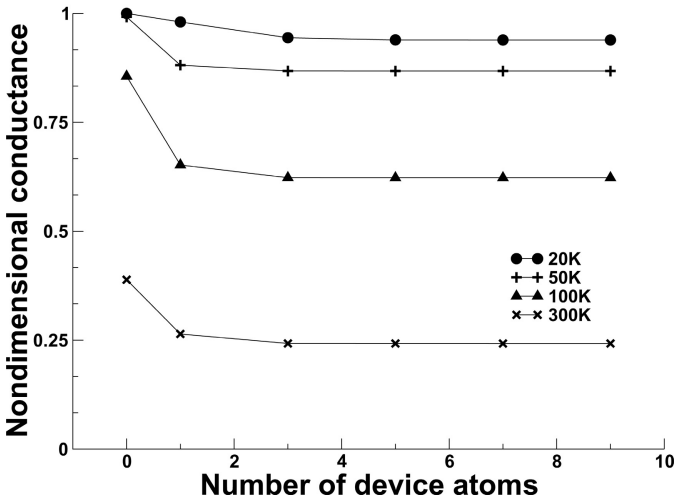

Figure 8. Length dependence of nondimensional thermal conductances at different temperatures. The case of zero number of device atoms represents the conductance of a homogeneous chain with "Contact" atomic properties.

in heterogeneous case 1 are plotted in Figure 8. The length of the device region is represented by the number of atoms. The case of zero number of device atoms represents a homogeneous atomic chain with "Contact" atom properties (atomic mass is 4.6×10^{-26} kg). The general trend of the nondimensional homogeneous conductance is that it decreases with increasing temperature, because higher temperatures shift the phonon spectrum to higher energies and reduce the integral in Eq. (36). The nondimensional heterogeneous conductance has a similar temperature dependence as that of the homogeneous chains. It also decreases as the length increases but levels out to an asymptotic value. In the ballistic transport regime, the length dependence of conductance is attributed mainly to the coupling and decoupling of phonon wave functions. If the "Device" is extremely short, phonons can easily propagate from one side to another.

CONCLUSIONS

A full derivation of the atomistic Green's function method and algorithmic details have been presented in this article. Numerical issues in the implementation of the AGF method have been addressed. Several examples illustrated the calculation of transmission functions, local and global density of states functions, and thermal conductances. The unique features of mesoscopic transport, such as Fabry-Perot peaks, are reproduced by this method. The ballistic thermal conductances for homogeneous and heterogeneous atomic chains, as well as their length dependencies, have been discussed. The AGF method can be further extended to simulate phonon transport in more sophisticated atomic structures. We expect that the presentation of the AGF method herein will make the method more accessible to researchers and will therefore motivate extended work on this useful approach.

REFERENCES

1. L. G. C. Rego and G. Kirczenow, Quantized Thermal Conductance of Dieletric Quantum Wires, *Phys. Rev. Lett.*, vol. 81, p. 232, 1998.
2. A. Ozpineci and S. Ciraci, Quantum Effects of Thermal Conductance through Atomic Chains, *Phys. Rev. B*, vol. 63, p. 125415, 2001.
3. P. Hyldgaard, Resonant Thermal Transport in Semiconductor Barrier Structures, *Phys. Rev. B*, vol. 69, p. 193305, 2004.
4. S. Pettersson and G. Mahan, Theory of the Thermal Boundary Resistance between Dissimilar Lattices, *Phys. Review B*, vol. 42, p. 7386, 1990.
5. R, Stoner and H. Maris, Kapitza Conductance and Heat Flow between Solids at Temperature from 50 to 300 K, *Phys. Rev. B*, vol. 48, p. 16373, 1993.
6. M. Cross and R. Lifshitz, Elastic Wave Transimission at an Abrupt Junction in a Thin Plate with Application to Heat Transport and Vibrations in Mesoscopic Systems, *Phys. Rev. B*, vol. 64, p. 85324, 2001.
7. D. Santamore and M. Cross, Effect of Surface Roughness on the Universal Thermal Conductance, *Phys. Rev. B*, vol. 63, p. 184306, 2001.
8. D. Santamore and M. Cross, Effect of Phonon Scattering by Surface Roughness on the Universal Thermal Conductance, *Phys. Rev. Lett.*, vol. 87, p. 115502, 2001.
9. D. Santamore and M. Cross, Surface Scattering Analysis of Phonon Transport in the Quantum Limit Using an Elastic Model, *Phys. Rev. B*, vol. 66, p. 144302, 2002.

10. K. Schwab, E. Henriksen, J. Worlock, and M. Roukes, Measurement of the Quantum of Thermal Conductance, *Nature*, vol. 404, p. 974, 2000.
11. W.-X. Li, K.-Q. Chen, W. Duan, J. Wu, and B.-L. Gu, Phonon Transport and Thermal Conductivity in Dielectric Quantum Wire, *J. Phys. D: Appl. Phys.*, vol. 36, p. 3027, 2003.
12. W.-Q. Huang, K.-Q. Chen, Z. Shuai, L. Wang, and W. Hu, Discontinuity Effect on the Phonon Transmission and Thermal Conductance in a Dielectric Quantum Waveguide, *Phys. Lett. A*, vol. 336, p. 245, 2005.
13. K.-Q. Chen, W.-X. Li, W. Duan, Z. Shuai, and B.-L. Gu, Effect of Defects on the Thermal Conductivity in a Nanowire, *Phys. Rev. B*, vol. 72, p. 45422, 2005.
14. D. Poulikakos, S. Arcidiacono, and S. Maruyama, Molecular Dynamics Simulation in Nanoscale Heat Transfer: A Review, *Microscale Thermophys. Eng.*, vol. 7, p. 181, 2003.
15. Z. Zhong, X. Wang, and J. Xu, Equilibrium Molecular Dynamics Study of Phonon Thermal Transport in Nanomaterials, *Numer. Heat Transfer B*, vol. 46, pp. 429–446, 2004.
16. S. Mazumdar and A. Majumdar, Monte Carlo Study of Phonon Transport in Solid Thin Films including Dispersion and Polarization, *J. Heat Transfer*, vol. 123, p. 749, 2001.
17. S. Srinivasan, R. Miller, and E. Marotta, Parallel Computation of the Boltzmann Transport Equation for Microscale Heat Transfer in Multilayered Thin Films, *Numer. Heat Transfer B*, vol. 46, pp. 31–58, 2004.
18. D. Angelescu, M. Cross, and M. Roukes, Heat Transport in Mesoscopic Systems, *Superlattices Microstruct.*, vol. 23, p. 673, 1998.
19. W. Little, The Transport of Heat between Dissimilar Solids at Low Temperature, *Can. J. Phys.*, vol. 37, p. 334, 1959.
20. E. Swartz and R. Pohl, Thermal Boundary Resistance, *Rev. Mod. Phys.*, vol. 61, p. 605, 1989.
21. R. Stevens, A. Smith, and P. Norris, Measurement of Thermal Boundary Conductance of a Series of Metal-Dielectric Interfaces by the Transient Thermoreflectance Technique, *J. Heat Transfer*, vol. 127, p. 315, 2005.
22. D. Ferry and S. Goodnick, *Transport in Nanostructures*, pp. 156–180, Cambridge University Press, New York, 1997.
23. S. Datta, *Electronic Transport in Mesoscopic Systems*, pp. 117–163, Cambridge University Press, New York, 1995.
24. S. Datta, *Quantum Transport: Atom to Transistor*, pp. 223–233, Cambridge University Press, New York, 2005.
25. W. Zhang, N. Mingo, and T. Fisher, Simulation of Phonon Interfacial Transport in Strained Silicon-Germanium Heterostructures, *J. Heat Transfer*, in press, 2007.
26. N. Mingo and L. Yang, Phonon Transport in Nanowires Coated with an Amorphous Material: An Atomistic Green's Function Approach, *Phys. Rev. B*, vol. 68, p. 245406, 2003.
27. N. Mingo and L. Yang, Erratum: Phonon Transport in Nanowires Coated with an Amorphous Material: An Atomistic Green's Function Approach [Phys. Rev. B 68, 245406 (2003)], *Phys. Rev. B*, vol. 70, p. 249901, 2004.
28. N. Ashcroft and N. Mermin, *Solid State Physics*, p. 439, Saunders College Publishers, Philadelphia, 1976.
29. A. Buldum, S. Ciraci, and C Fong, Quantum Heat Transfer through an Atomic Wire, *J. Phys. Condensed Matters*, vol. 12, p. 3349, 2000.
30. F. Guinea, C. Tejedor, F. Flores, and E. Louis, Effective Two-Dimensional Hamiltonian at Surfaces, *Phys. Rev. B*, vol. 28, p. 4397, 1983.
31. G. Golub and C. V. Loan, *Matrix Computations*, 3rd ed., p. 152, The John Hopkins University Press, Baltimore, MD, 1996.
32. M. Lannoo and P. Friedel, *Atomic and Electronic Structure of Surfaces*, pp. 42–48, Springer-Verlag, Berlin, 1991.
33. C. Kittel, *Introduction to Solid State Physics*, 8th ed., p. 108, Wiley, New York, 2005.